Qian, S. and Bau, H., H., 2003, A Mathematical Model of Lateral Flow Bio-Reactions Applied to Sandwich Assays, Analytical Biochemistry, 322, 89-98

A MATHEMATICAL MODEL OF LATERAL FLOW BIO-REACTIONS APPLIED TO SANDWICH ASSAYS

Shizhi Qian and Haim H. Bau*
Department of Mechanical Engineering and Applied Mechanics,
University of Pennsylvania
Philadelphia, PA 19104-6315

ABSTRACT

Lateral flow (LF) bio-detectors facilitate low-cost, rapid identification of various analytes at the point of care. The LF cell consists of a porous membrane containing immobilized ligands at various locations. Through the action of capillary forces, samples and reporter particles are transported to the ligand sites. The LF membrane is then scanned or probed, and the concentration of reporter particles is measured. A mathematical model for sandwich assays is constructed and used to study the performance of the LF device under various operating conditions. The model provides insights into certain experimental observations including the reduction in the level of the detected signal at high target analyte concentrations. Furthermore, the model can be used to test rapidly and inexpensively various operating conditions, assist in the device's design, and optimize the performance of the LF device.

Key words: lateral flow test, lateral flow immunoassay, point of care testing, immunoassay test strips

* All correspondence should be addressed to this author, bau@seas.upenn.edu

1. Introduction

In recent years, there has been a growing interest in developing low-cost techniques for rapid identification of analytes and pathogens at the point of care. One such technique utilizes lateral-flow (LF) reactors[1-14]. There are many examples of the application of LF reactors in the health care industry. Here we list just a few examples such as home pregnancy tests; human fecal occult blood detection; HIV-1 diagnostics; mycobacterium tuberculosis diagnostics; and the detection of drugs of abuse. The LF cell consists of a porous membrane or strip that is often made out of nitrocellulose. Antibodies and/or ogligonucleotides are immobilized at predetermined locations on the membrane. The target analytes are mixed with pre-engineered reporter particles such as colloidal gold, carbon black, dyed polystyrene, or phosphor. In this paper, we focus on situations in which the reporter particles are mixed with the sample prior to their introduction into the membrane.

In the sandwich assay format, the sample is mixed with the reporter particles. Some of the target analytes bind to the particles and some remain free in the solution. By the action of capillary forces, both the particle-bound analytes and free analytes migrate up the LF membrane and through the sites where ligands are immobilized (capture zones). Both particle-bound analytes and the free analytes bind to the ligands. After some time, the LF strip is analyzed, and the concentration of the reporter particles is measured as a function of location. It is also possible to obtain the reporter particle concentration as a function of time.

Although LF immunoassay technology is widely used in the healthcare industry, in home care, and in the monitoring of the quality of the water and food supply, the format suffers from certain shortcomings such as signal saturation and eventual decline when the target analyte concentration increases. It would be desirable to have a predictive, design tool that would allow

one to test rapidly and inexpensively the effects of various design parameters.

The objective of this paper is to provide a mathematical model that allows one to predict kinetic characteristics. In addition to providing insights into device operation, such a model also enables one to optimize device performance.

2. MATHEMATICAL MODEL

We consider a lateral flow (LF) reactor that consists of a flat, porous membrane[9-19]. A schematic description of the LF reactor is diagrammed in Fig 1. A sample containing the target analytes, reporter particles, and buffer solution is introduced in a reservoir that is in contact with a dry porous membrane (typically made of nitrocellulose). The solution flows through the membrane by capillary action.

Ligands are immobilized at various locations in the membrane. The membrane may contain many capture zones; each designed to bind specifically with a target analyte. As the solution passes through the capture zones, both analytes bound to reporters and free analytes interact with the ligands. Subsequent to the binding process, the concentration of reporter particles is measured as a function of location[12-13, 16]. When specific target analytes are present in the solution, the concentration of reporter particles and the signal generated at the corresponding capture sites will be higher than away from the capture zone. Since the locations of the capture sites are known, one can determine whether the specific target analytes are present in the sample. Ideally, the signal's magnitude would be proportional to the target analyte's concentration. We will see later in the paper that this is not always the case.

We assume that the solution is dilute and contains various target analytes A_i. The analytes interact with the reporter particles to form particle-analyte complexes, $A_i + P \leftrightarrows PA_i$. Free

analytes of type *i* (A_i) as well as reporter-bound analytes (PA_i) interact with the immobilized ligands of type *i* (R_i) to form the complexes RA_i ($A_i+R_i \leftrightarrows RA_i$) and RPA_i ($PA_i+R_i \leftrightarrows RPA_i$), respectively. Additionally, unbound particles (P) may bind to the complex (RA_i) to form the complex RPA_i ($P+RA_i \leftrightarrows RPA_i$). In the above, we assume first order reversible interactions. The analysis can be readily extended to include more complicated interactions.

For simplicity, we consider below the particular case of a single target analyte. Hereafter, we drop the subscript *i*. We use square brackets to denote the concentrations of the various species. In other words, [A], [P], [R_0], [PA], [RA], [RPA] are, respectively, the concentrations of the free analyte, free particles, total ligand, particle-analyte complex, ligand-analyte complex, and ligand-analyte-particle complex. The concentrations are functions of space and time, i.e., [A](**x**,t), where **x** is the space coordinate and t is time.

The rate of formation (F_{PA}) of the particle-analyte complex (PA) is proportional to the product of the free analytes ([A]) and free particles ([P]).

$$F_{PA} = k_{a1}[A][P] - k_{d1}[PA]. \tag{1}$$

The rate of formation (F_{RA}) of the ligand-analyte complex (RA) is:

$$F_{RA} = k_{a2}[A]([R_0] - [RA] - [RPA]) - k_{d2}[RA] - k_{a4}[RA][P] + k_{d4}[RPA]. \tag{2}$$

To keep track of the rate of formation (F_{RPA}) of the complex RPA, it is convenient to monitor separately the rate of formation of RPA due to the interactions ($P_i+R \leftrightarrows RPA$) and ($P+RA \leftrightarrows RPA$).

$$F_{RPA} = F^{1}{}_{RPA} + F^{2}{}_{RPA}, \tag{3}$$

where

$$F^{1}{}_{RPA} = k_{a3}[PA]([R_0] - [RA] - [RPA]) - k_{d3}[RPA] \tag{4}$$

and

$$F^{2}{}_{RPA} = k_{a4}[RA][P] - k_{d4}[RPA]. \quad (5)$$

In the above, k_{aj} and k_{dj} are, respectively, the appropriate association and dissociation rate constants; and $[R_0]$-[*RA*]-[*RPA*] is the concentration of the unbound ligand.

Typically, the porous membrane is narrow and thin. The sample propagates as a slug with a nearly sharp liquid-air interface and average velocity U, and the ligands are immobilized uniformly in the section $x_{L1}<x<x_{L2}$. Consequently, we need to consider only one space dimension (x) that is aligned along the membrane's length. To the first order approximation, we assume that the particles move at the solution's speed and that particles do not get trapped in the porous matrix.

The concentrations of the free target analyte (*[A](x, t)*), the particle-analyte complex (*[PA](x,t)*), the free particles (*[P](x,t)*), the ligand-analyte complex (*[RA](x,t)*, and the ligand-analyte-particle complex ([*RPA*]) are described, respectively, by the convection-diffusion-reaction equations:

$$\frac{\partial[A]}{\partial t} = D_A \frac{\partial^2[A]}{\partial x^2} - U\frac{\partial[A]}{\partial x} - (F_{PA} + F_{RA}), \quad (6)$$

$$\frac{\partial[PA]}{\partial t} = D_P \frac{\partial^2[PA]}{\partial x^2} - U\frac{\partial[PA]}{\partial x} + (F_{PA} - F^{1}{}_{RPA}), \quad (7)$$

$$\frac{\partial[P]}{\partial t} = D_P \frac{\partial^2[P]}{\partial x^2} - U\frac{\partial[P]}{\partial x} - \left(F_{PA} + F^{2}_{RPA}\right), \quad (8)$$

$$\frac{\partial[RA]}{\partial t} = F_{RA}, \quad (9)$$

and

$$\frac{\partial[RPA]}{\partial t} = F_{RPA}. \quad (10)$$

In the above, D_A and D_P are, respectively, the molecular diffusion coefficients of the analyte and the particles. $D_A \sim 1.0\times10^{-10}$ m^2/s and $D_P \sim 1.0\times10^{-12}$ m^2/s are estimated from the Stokes-Einstein equation. [*RA*] and [*RPA*] exist only in the capture zone and are equal to zero elsewhere.

In our calculations, we use the average fluid velocity of U~0.2 mm/s which we obtained from experimental data. Time-dependent velocities can be readily incorporated into the model.

We consider the case when the reporter particles are premixed with the sample prior to their introduction into the membrane. Specifically, a sample containing, respectively, concentrations $[A_0]$ and $[P_0]$ of the target analyte and reporter particles is introduced into a chamber that is in contact with the membrane. Since the reporter particles and target analytes are premixed, the interaction $A+P \leftrightarrows PA$ may take place prior to entry into the membrane. Thus, the sample entering the membrane consists of free target analytes (*A*), free reporter particles (*P*), and an particle-analyte complex (*PA*). The concentration of each of the above depends on the residence time and stirring conditions in the sample chamber. Since these conditions may vary from one case to another, we consider here two extreme cases. In the first instance, we assume that the mixture of the target analyte and reporter particles was allowed sufficient time to equilibrate prior to entering the membrane. We refer to this case as premixed and equilibrated (**PME**). The corresponding equilibrium concentrations are denoted with the subscript *e*:

$$PA_e = \frac{1}{2}\left([A_0] + [P_0] + \frac{k_{d1}}{k_{a1}} - \sqrt{\left([A_0] + [P_0] + \frac{k_{d1}}{k_{a1}} \right)^2 - 4[A_0][P_0]} \right), \tag{11}$$

$$A_e = A_0 - PA_e, \tag{12}$$

and

$$P_e = P_0 - PA_e. \tag{13}$$

Thus, the inlet conditions at x=0 are:

$$[A](0,t)=A_e H(T-t),\ [P](0,t)=P_e\, H(T-t),\ \text{and}\ [PA](0,t)=PA_e\, H(T-t). \tag{14}$$

The sample flow through the membrane takes place over the time interval $0<t<T$. T is determined by the amount of sample and the size of the sink (absorption pad) at the membrane's downstream end. In the above,

$$H(\xi)=\begin{cases}0 & \xi \le 0\\ 1 & \xi > 0\end{cases} \tag{15}$$

is the Heaviside step function.

In the second extreme case, we assume that the mixture spent limited time in a poorly stirred chamber and that no interactions between the target analyte and reporter particles took place. In other words, the mixture entering the membrane does not contain any complex PA. We refer to this case as premixed and unequilibrated (**PMU**). In this case, at x=0,

$$[A](0,t)=A_0\, H(T-t),\ [P](x,0)=P_0\, H(T-t),\ \text{and}\ [PA](x,0)=0. \tag{16}$$

In the **PMU** case, PA will form as the mixture migrates through the membrane and a mixture of A, P, and PA will enter the capture zone. The concentration of PA may, however, be below the corresponding equilibrium concentration.

The initial conditions for both cases are:

$$[P](x,0)=[PA](x,0)=[RA](x,0)=[RPA](x,0)=0 \tag{17}$$

and

$$R(x,0)=\begin{cases}R_0 & \left(x_{L1}<x<x_{L2}\right)\\ 0 & otherwise\end{cases}. \tag{18}$$

Finally, at the membrane's exit ($x=L$), we specify the customary outflow conditions:

$$\frac{\partial [A](L,t)}{\partial x}=\frac{\partial [P](L,t)}{\partial x}=\frac{\partial [PA](L,t)}{\partial x}=0. \tag{19}$$

Given the low magnitude of the diffusion coefficients, the outflow boundary conditions are not likely to have any significant effect on the model's predictions.

We also consider the simplified, special case of a well-mixed capture zone (**PMW**). When the flow rate is relatively high, the various species are nearly uniformly distributed in space ($\frac{\partial}{\partial x} = 0$) and the interactions in the capture zone have little effect on the concentrations of the target analyte and the analyte-particle complex. Furthermore, when the capture zone is located sufficiently far downstream from the membrane's entrance, one may assume equilibrium conditions. In other words, at the inlet to the capture zone, we have $[A]=A_e$, $[P]=P_e$, and $[PA]=PA_e$. The corresponding equilibrium concentrations were given in equations 11-13. We assume that these concentrations are maintained throughout the capture zone. Thus, the well-mixed case (**PMW)** is the limiting case of the premixed and equilibrated case (**PME)** when the flow rate is high.

It is instructive to consider this idealized case since it allows us to reduce the partial differential equations to algebraic equations. Unfortunately, the algebraic system is too complicated to allow for the derivation of closed form expressions. In order to derive relatively simple expressions for the equilibrium concentrations of the ligand-analyte (*RA*) and ligand-analyte-particle (*RPA*) complexes, we consider the special case of $k_{a4}=k_{d4}=0$.

In the well-mixed capture zone (**PMW**), the equilibrium concentrations of the ligand-analyte-particle (*RPA*) and ligand-analyte (*RA*) are, respectively,

$$[RPA] = \frac{k_{a3}k_{d2}[R_0][PA_e]}{k_{d2}(k_{d3} + k_{a3}[PA_e]) + k_{a2}k_{d3}[A_e]} \tag{20}$$

and

$$[RA] = \frac{k_{a2}k_{d3}[R_0][A_e]}{k_{d2}(k_{d3} + k_{a3}[PA_e]) + k_{a2}k_{d3}[A_e]}. \quad (21)$$

Away from the capture zone, [*RPA*]=[*RA*]=0.

The total particle concentration is typically detected with a scanner. The scanner measures either the fluorescent or phosphor emission intensity or color intensity. In the capture zone, the signal is proportional to *S*=[*P*]+[*PA*]+[*RPA*]. Away from the capture zone, the signal is proportional to S_0=[*P*]+[*PA*]=[P_0]. We consider S_0 as the background signal and define the amplitude $\Delta S = S - S_0$ and the contrast index $DS = \frac{S - S_0}{S_0}$.

In the well-mixed case (PMW), $DS = \frac{[RPA]}{[P_0]}$. When the target analyte concentration ([A_0]) is small,

$$\mathrm{DS} \sim \frac{k_{a1}k_{a3}[R_0][P_0]}{k_{d3}(k_{a1}[P_0] + k_{d1})}[A_0] \quad (22)$$

increases nearly linearly as the target analyte concentration increases. Unfortunately, this is not true when the target analyte concentration is relatively large (See section 3).

Another interesting limit corresponds to very large [P_0]. When [P_0] is sufficiently large, the equilibrium concentrations of *PA* and *RPA* become independent of [P_0] and so does the signal *S*. When P_0 is large, increases in [P_0] will cause a reduction in the contrast index *DS*.

3. RESULTS AND DISCUSSION

To illustrate the capabilities of the mathematical modeling, the convection-diffusion-reaction equations were solved numerically using the finite element program Femlab™. Unless

otherwise stated, the results correspond to $k_{a1}= k_{a2} = k_{a3}= k_{a4}=10^6$ (1/MS), $k_{d1}=k_{d2}=k_{d3}=k_{d4}=10^{-3}$ (1/s), $[P_0]=[R_0]=[A_0]$=10nM, L=0.041m, $x_{L1}=L/2$, $x_{L2}=3L/4$, and $U=2\cdot10^{-3}$m/s.

Fig. 2 depicts the sequence of events when the analyte and reporter particles are pre-mixed and equilibrated prior to their introduction into the membrane (case **PME**). The mixture that enters the membrane contains $[A]$=2.7nM, $[P]$=2.7nM, and $[PA]$=7.3nM. The concentration of this mixture remains unaltered until its arrival at the capture zone. We assume that a sufficient amount of analyte is available to eventually achieve equilibrium conditions in the capture zone. The figure depicts the signal $S=[P]+[PA]+[RPA]$ as a function of the location x at various times t=4 (a), 5(b), 6(c), 7(d), 8(e), and 9 (f) minutes. Time t=0 corresponds to the time when the solution started flowing up the membrane. By the time t=4 minutes, the solution has transversed the entire length of the membrane (Fig. 2a). Upstream of the capture zone, the particle concentration is equal to the initial particle concentration, and therefore the signal $S=S_0=[P]+[PA]=[P_0]$ is not a function of x ($[RPA]$=0 away from the capture zone). We refer to S_0 as the baseline. Due to the interactions between the particle-analyte complex and the immobilized ligands, the concentration of the particles in the capture zone increases gradually over time until equilibrium conditions are established. Since some of the reporter particles are retained in the capture zone, initially, the particle concentration downstream of the capture zone is smaller than upstream of the capture zone. This downstream concentration increases, however, as time increases, and once equilibrium conditions are established, it is equal to the particle concentration (S_0) upstream of the capture zone. The elevated particle concentration $\Delta S=S-S_0$ in the capture zone indicates the presence of the target analyte in the sample. One might anticipate that the magnitude of ΔS would be proportional to the target analyte's concentration in the sample.

Fig. 3 depicts the sequence of events when the target analyte and reporter particles are pre-mixed but not equilibrated prior to their introduction into the membrane (case **PMU**). We again assume that a sufficient amount of analyte is available for equilibrium conditions to be established in the capture zone. The concentrations of the various species at the membrane's inlet are $[A]=[A_0]$, $[P]=[P_0]$, and $[PA]=0$. As the mixture transverses along the membrane, the target analye interacts with the reporter particles to form *PA*. There is insufficient time for equilibrium conditions to be established, and the composition of the mixture at the inlet to the capture zone is: $[A]$=5.4nM, $[P]$=5.4nM, and $[PA]$=4.6nM. When the distance from the membrane inlet to the capture zone is shortened and/or the flow rate is increased, the *PA* concentration at the capture zone's inlet will decrease. Conversely, when the distance from the membrane's inlet to the capture zone is lengthened and/or the flow rate is decreased, the *PA* concentration at the capture zone's inlet will approach the corresponding equilibrium value.

To illustrate the above statements more clearly, Fig. 4 depicts the concentration of *PA* as a function of *x* for the premixed and equilibrated (**PME**, dash lines), premixed and unequilibrated (**PMU**, dash-dot lines) and well-mixed (**PMW**, solid line) cases at various times *t*=4, 6, 8, and 10 minutes. In the well-mixed case (**PMW**), $[PA]$ is independent of x, and it is constant along the entire length of the membrane. In the equilibrium pre-mixed case (**PME**), $[PA]$ is constant upstream of the capture zone ($x<x_{L1}$), and it decreases in the capture zone as *x* increases because *PA* binds with the ligand to form the complex *RPA*. Downstream of the capture zone ($x>xL_2$), $[PA]$ may further decrease as *x* increases. Since the target analyte binds to ligands in the capture zone, the free target analyte concentration in the mixture decreases, and this triggers the dissociation of *PA* into free particles (*P*) and free analyte (*A*) and the reduction in the *PA* concentration. With increased time, the concentration of *PA* both in the capture and

downstream zones increases and eventually (at about t=10 minutes) reaches the levels of the **PMW** case. Finally, we consider the **PMU** case. In the PMU case, the concentration of *PA* at the membrane's entrance is equal to zero. As the reporter particles and target analyte flow side by side, the concentration of the complex *PA* increases gradually. Depending on the length of the membrane upstream of the capture zone, *PA* may or may not achieve equilibrium conditions. In the example depicted in Fig. 4, equilibrium conditions were not established. Thus, the concentration of *PA* at the capture zone inlet is smaller than in the premixed and equilibrated (**PME)** case. Once the mixture enters the capture zone, initially the *PA* concentration decreases as x increases; but, once sufficient time has gone by, this trend is reversed.

Next, we examined the kinetics of the binding process. To this end, we calculated the average total reporter particle concentration in the capture zone $\overline{S}(t) = \frac{1}{x_{L2} - x_{L1}} \int_{x_{L1}}^{x_{L2}} S(x,t)dx$ as a function of time. Fig. 5 depicts $\overline{S}(t)$ as a function of time for the same conditions as in Figs. 2 and 3. There is no signal before the sample mixture arrives at the interaction zone. Once the mixture arrives, the signal's intensity increases as time increases. Eventually, the signal saturates. If one is interested only in the maximum intensity of the signal, one should allow sufficient time for "signal development." Fig. 5 illustrates the "penalty" that one would incur when the LF reactor is scanned prematurely.

Finally, we examine the contrast index, $DS = (\overline{S} - S_0)/S_0$, as a function of the target analyte, the receptor particles, and the ligand concentrations. Fig. 6 depicts DS as a function of the target analyte concentration ($[A_0]$) on a log-log scale when $k_{a1}= k_{a2}= k_{a3}= k_{a4}=10^6$ (1/MS), $k_{d1}=k_{d2}=k_{d3}=k_{d4}=10^{-3}$ (1/s), $[P_0]$=10nM, and $[R_0]$=10nM. The line with the square symbols, the line with the triangles, and the solid line correspond, respectively, to the premixed and

equilibrated (**PME)**, premixed and unequlibrated (**PMU)**, and well-mixed (**PMW)** cases. Similar qualitative behavior is observed in all these three cases. When the target analyte concentration ([A_0]) is relatively small, *DS* increases nearly linearly as a function of [A_0]. This is consistent with the predictions of equation 22, and is the desired behavior. As the target analyte concentration increases further, *DS* attains a maximum at target analyte concentration [A_{0c}] and then decreases. Users of LF are familiar with this unfortunate phenomenon, and refer to it as "sensor poisoning." The reason for the leveling and eventual decrease in the signal's magnitude is that at high concentrations, the analyte binds both to the reporter particles and to the ligands and blocks many of the particle-analyte complexes from binding with the ligands. The signal's amplitude exhibits similar behavior to that of the contrast index. Fig. 7 depicts $\Delta S = \overline{S} - S_0$ as a function of the target analyte concentration [A_0]. The target analyte concentration at which the signal intensity levels off depends, of course, on other system parameters such as the total ligand concentration. An increase in the ligand concentration (not shown here) will shift the maximum in the curve to the right. The system designer should therefore adjust the ligand concentration according to the expected target analyte concentrations. Fig. 7's predictions are in qualitative agreement with experimental observations (see Fig. 2C in [12] and Fig.4 in [19]). Since the rate constants of the experiments are not known, rigorous quantitative comparison with the experimental data is not possible. Nevertheless, to verify that the predicted trends are similar to the ones observed in experiments, Fig. 8 depicts the normalized signal $\left(\overline{S} - S_0\right)/\left(\overline{S}_{\max} - S_0\right)$ as a function of the normalized target analyte concentration [A_0]/[A_{0c}], where [A_{0c}] corresponds to the analyte concentration at the signal's peak. The solid line, dashed line, circles, upright triangles, and inverted triangles correspond, respectively, to premixed unequlibrated (PMU) model predictions, well-mixed (PMW) model predictions, experimental data from Fig. 2c in [12],

experimental data from Fig. 4 (SR membrane) in [19] and experimental data from Fig. 4 (SX membrane) in [19]. The theoretical predictions are in good agreement with the experimental observations.

Next, the effect of the reporter particle concentration ($[P_0]$) on the sensor signal was evaluated. Fig. 9 depicts *DS* as a function of the reporter particle concentration ($[P_0]$) on a log-log scale when $k_{a1}= k_{a2}= k_{a3}= k_{a4}=10^6$ (1/MS), $k_{d1}=k_{d2}=k_{d3}=k_{d4}=10^{-3}$ (1/s), $[A_0]$=10nM, and $[R_0]$=10nM. The line with the square symbols, the line with the triangles, and the solid line correspond, respectively, to the premixed and equilibrated (**PME)**, premixed and unequlibrated (**PMU)**, and well-mixed (**PMW)** cases. Similar qualitative behavior is observed in all three cases. When the reporter particle concentration is relatively small, *DS* appears to be nearly independent of $[P_0]$. In other words, *DS* appears as a horizontal line. This behavior can be attributed to both *S* and S_0 increasing at a similar rate as $[P_0]$ increases. Once the reporter particle concentration exceeds a critical value, further increases in $[P_0]$ lead to a decrease in the contrast index *DS*. This is due to the fact that for relatively large $[P_0]$, *S* increases at a slower than linear rate as $[P_0]$ increases. This can be seen more clearly in Fig. 10, which depicts $\Delta S = \overline{S} - S_0$ as a function of $[P_0]$. At low P_0 concentrations, ΔS increases nearly linearly as $[P_0]$ increases. Once a critical value ($[P_{0c}]$) has been exceeded, ΔS achieves a plateau. This phenomenon is due to the fact that the ligands have a limited binding capacity. At relatively low concentrations, increasing the inventory of reporter particles increases the concentration of particle-analyte-ligand complexes and contributes to the signal. Once the binding capacity of the ligands has been saturated, further increases in the concentration of reporter particles do not add to $(S - S_0)$, and the contrast index decreases. Somewhat surprisingly, the signal level in the premixed and unequlibtaed (**PMU)** case is a bit higher then in the premixed and equilibrated

(**PME)** case. This is due to the fact that in the PMU case, the PA concentration is smaller (see Fig. 4) and fewer reporter particles are excluded from binding to the RA complex. The theoretical predictions of Fig. 10 resemble qualitatively the experimental curves examining the effect of reporter particle concentration on signal level (see Fig. 2B in [12]). Fig. 11 compares the theoretical predictions with experimental observations. The figure depicts the normalized signal $\left(\overline{S}-S_0\right)/\left(\overline{S}_{\max}-S_0\right)$ as a function of the normalized reporter particle concentration $[P_0]/[P_{0c}]$, where $[P_{0c}]$ corresponds to the critical reporter particle concentration. The solid line, dashed line, and circles, correspond, respectively, to PMU model predictions, PMW model predictions, and experimental data from Fig. 2B in [12]. The theoretical predictions are in good agreement with the experimental observations.

Finally, we examine the effect of the ligand concentration on the contrast index *DS*. Fig. 12 depicts DS as a function of $[R_0]$ on a log-log scale when $k_{a1}= k_{a2}= k_{a3}=k_{a4}=10^6$ (1/MS), $k_{d1}=k_{d2}=k_{d3}=k_{d4}=10^{-3}$ (1/s), $[A_0]$=10nM, and $[P_0]$=10nM. The line with the square symbols, the line with the triangles, and the solid line correspond, respectively, to the **PME**, **PMU**, and **PMW** cases. Similar qualitative behavior is observed in all these three cases. Not surprisingly, as $[R_0]$ increases, *DS* linearly increases.

4. Conclusions

We introduced a mathematical model to investigate the performance of a LF device under varying operating conditions. The model predictions favorably agree with experimental observations. The major conclusions are:

(i) When the target analyte concentration is low, the signal level increases nearly linearly as the target analyte concentration increases. This, however, is not true at high target

analyte concentrations. Once the target analyte concentration exceeds a certain value, the signal peaks and then declines. The magnitude of this critical value is, among other things, a function of the immobilized ligand and reporter particle concentrations, and the reaction rates constants.

(ii) There is a critical concentration of reporter particles. Below this critical value, as the reporter particle concentration increases so does the signal's amplitude without an adverse effect on the contrast index. Further increases in the reporter particle concentration above this critical value do not lead to any increases in the signal amplitude and have a detrimental effect on the contrast index.

(iii) It is desirable to maintain a ligand concentration close to or above a certain critical value so as to maximize the signal's amplitude and the contrast index.

(iv) The magnitude of the interaction between the target analyte and reporter particles prior to their entry into the membrane has a relatively minor impact on signal amplitude.

The model can be augmented in different ways such as by simulating particle trapping, allowing for time-dependent flow rates, and accommodating small samples that do not allow for equilibrium conditions to be established. We have not included these effects here because of the lack of relevant experimental data. We hope that the model presented here will be useful for the design and optimization of LF sensors operating with sandwich assays. Moreover, the model allows one to test rapidly and inexpensively the effects of various parameters and operating conditions on sensor performance.

ACKNOWLEDGMENTS

The work described in this paper was supported, in part, by DARPA's SIMBIOSYS program (Dr. Anantha Krishnan, program director) and by NIH grant 1U01 DE 14964-01.

REFERENCES

[1] C. Barrett, C. Good, C. Moore, Comparison of point-of-collection screening of drugs of abuse in oral fluid with a laboratory-based urine screen, Forensic Science International, 122 (2001) 163-166

[2] A. Jehanli, S. Brannan, L. Moore, V.R. Spiehler, Blind trials of an onsite saliva drug test for marijuana and opiates, Journal of Forensic Sciences, 46 (2001) 1214-1220

[3] Y. Oku, K. Kamiya, H. Kamiya,Y. Shibahara, T. Ii, Y. Uesaka, Development of oligonucleotide lateral-flow immunoassay for multi-parameter detection, Journal of Immunological Methods, 258 (2001) 73-84

[4] M. Lonnberg, J. Carlsson, Quantitaive Detection in the Attomole Range for Immunochromatographic tests by Means of a Flatbed Scanner, Analytical Biochemistry, 293(2001) 224-231

[5] H.L. Smits, C.K.Eapen, S. Sugathan, M. Kuriakose, M.H. Gasem, C.Yersin, D. Sasaki, B. Pujianto, M. Vestering, T.H. Abdoel, G.C. Gussenhoven, Lateral-flow assay for rapid serodiagnosis of human leptospirosis, Clinical and Diagnostic Laboratory Immunology, 8 (2001) 166-169

[6] F. Ketema, C. Zeh, D.C. Edelman, R. Saville, N.T. Constantine, Assessment of the performance of a rapid, lateral flow assay for the detection of antibodies to HIV, Journal of Acquirer Immune Deficiency Syndromes, 27 (2001) 63-70

[7] F.E. Ahmed, Detection of genetically modified organisms in foods, Trends in

Biotechnology, 20 (2002) 215-223

[8] Y. Al-Yousif, J. Anderson, C. Chard-Bergstrom, S. Kapil, Development, evaluation, and application of lateral-flow immunoassay (immunochromatography) for detection of rotavirus in bovine fecal samples, Clinical and Diagnostic Laboratory Immunology, 9 (2002) 723-724

[9] C. Quach, D. Newby, G. Daoust, E. Rubin, J. McDonald, QuickVue influenza test for rapid detection of influenza A and B viruses in a pediatric population, Clinical and Diagnostic Laboratory Immunology, 9 (2002) 925-926

[10] J. Tao, N. DelosSantos, C. Dou, One step lateral flow immunoassay for detection of Ecstasy in human urine, Clinical Chemistry, 48 (2002) B14 Part 2

[11] A. Salomone, P. Roggero, Host range, seed transmission and detection by ELISA and lateral flow of an Italian isolate of Pepino mosaic virus, Journal of Plant Pathology, 84 (2002) 65-68

[12] P. Corstjens, M. Zuiderwijk, M. Nilsson, H. Feindt, R. S. Niedbala, H. J.Tanke, Lateral-Flow and Up-Converting Phosphor Reporters to Detect Single-Stranded Nucleic Acids in Sandwich-Hybridization Assay, Analytical Biochemistry, 312(2003)191-200

[13] P. Corstjens , M. Zuiderwijk, A. Brink, S. Li, H. Feindt, R.S. Neidbala, H. Tanke, Use of up-converting phosphor reporters in lateral-flow assays to detect specific nucleic acid sequences: A rapid, sensitive DNA test to identify human papillomavirus type 16 infection, Clinical Chemistry, 47 (2001) 1885-1893

[14] S.P. Johnston, M.M. Ballard, M.J. Beach, L. Causer, P.P. Wilkins, Evaluation of three commercial assays for detection of giardia and cryptosporidium organisms in fecal specimens, Journal of Clinical Microbiology, 41 (2003) 623-626

[15] W.K. Fong, Z. Modrusan, J.P. McNevin, J. Marostenmaki, B. Zin, F. Bekkaoui, Rapid solid-phase immunoassay for detection of methicillin-resistant Staphylococcus aureus using cycling probe technology, Journal of Clinical Microbiology, 38 (2000) 2525-2529

[16] R.S. Niedbala, H. Feindt, K. Kardos, T. Vail, J. Burton, B. Bielska, S. Li, D. Milunic, P. Bourdelle, R.Vallejo, Detection of analytes by immunoassay using up-converting phosphor technology, Analytical Biochemistry, 293 (2001) 22-30

[17] M. Lonnberg, J. Carlsson, Chromatographic performance of a thin microporous bed of nitrocellulose, Journal of Chromatography B-Analytical Technologies in the Biomedical and Life Sciences, 763 (2001) 107-120

[18] H.H. Weetall, K.R. Rogers, A simple assay for 2,4-dichlorophenoxyacetic acid using coated test-strips, Analytical Letters, 35 (2002) 1341-1348

[19] J. Hampl, M. Hall, N.A. Mufti, Y.M. Yao, D.B. MacQueen, W. H. Wright, D.E. Cooper, Upconverting Phosphor Reporters in Immunochromatographic Assays, Analytical Biochemistry, 288(2001) 176-187

Lists of Captions:

1. A schematic description of the lateral flow bio-detector. A mixture of target analyte A and reporter particles P migrate by capillary force up the membrane towards the capture zone where ligands are immobilized.

2. The signal S as a function of the spatial coordinate x when a pre-mixed solution at equilibrium conditions is introduced into the membrane. $k_{a1}=k_{a2}=k_{a3}= k_{a4}=10^6$ (1/MS), $k_{d1}=k_{d2}=k_{d3}=k_{d4}=10^{-3}$ (1/s), $[A_0]=[P_0]= [R_0]$=10nM. t=4(a), 5(b), 6(c), 7(d), 8(e), and 9(f) min.

3. The signal S as a function of the spatial coordinate x when a non-equilibrium, pre-mixed solution is introduced into the membrane. $k_{a1}=k_{a2}=k_{a3}= k_{a4}=10^6$ (1/MS), $k_{d1}=k_{d2}=k_{d3}=k_{d4}=10^{-3}$ (1/s), and $[A_0]=[P_0]= [R_0]$=10nM. t=4(a), 5(b), 6(c), 7(d), 8(e), and 9(f) min.

4. The concentration $[PA]$ as a function of x for **PME** (dash lines), **PMU** (dash-dot lines) and **PMW** (solid line) conditions. $k_{a1}=k_{a2}=k_{a3}= k_{a4}=10^6$ (1/MS), $k_{d1}=k_{d2}=k_{d3}=k_{d4}=10^{-3}$ (1/s), and $[A_0]=[P_0]= [R_0]$=10nM.

5. The average concentration $\overline{S}$ in the capture zone as a function of time for equilibrium pre-mixed (solid line) and non-equilibrium pre-mixed (dashed line) conditions. $k_{a1}=k_{a2}=k_{a3}= k_{a4}=10^6$ (1/MS), $k_{d1}=k_{d2}=k_{d3}=k_{d4}=10^{-3}$ (1/s), and $[A_0]=[P_0]= [R_0]$=10nM.

6. The contrast index DS as a function of the target analyte concentration. $k_{a1}=k_{a2}=k_{a3}= k_{a4}=10^6$ (1/MS), $k_{d1}=k_{d2}=k_{d3}=k_{d4}=10^{-3}$ (1/s), $[P_0]$=10nM, and $[R_0]$=10nM. The solid line, dot line (with squares) and dashed line (with Δ) denote, respectively, the predictions of the well-mixed model, the equilibrium pre-mixed model, and the non-equilibrium pre-mixed model.

7. The signal's amplitude $S-S_0$ as a function of the target analyte concentration. $k_{a1}=k_{a2}=k_{a3}= k_{a4}=10^6$ (1/MS), $k_{d1}=k_{d2}=k_{d3}=k_{d4}=10^{-3}$ (1/s), $[P_0]$=10nM, and $[R_0]$=10nM. The solid line, dot line

(with squares) and dashed line (with Δ) denote, respectively, the predictions of the well-mixed model, the equilibrium pre-mixed model, and the non-equilibrium pre-mixed model.

8. The normalized signal $\left(\overline{S}-S_0\right)/\left(\overline{S}_{\max}-S_0\right)$ is depicted as a function of the normalized target analyte concentration $[A_0]/[A_{0c}]$. The solid line, dashed line, circles, upright triangles, and inverted triangles correspond, respectively, to premixed and unequlibrated (**PMU)** model predictions, well-mixed (**PMW)** model predictions, experimental data from Fig. 2c in [12], experimental data from Fig. 4 (SR membrane) in [19] and experimental data from Fig. 4 (SX membrane) in [19].

9. The contrast index *DS* as a function of the reporter particles' concentration. $k_{a1}=k_{a2}=k_{a3}=k_{a4}=10^6$ (1/MS), $k_{d1}=k_{d2}=k_{d3}=k_{d4}=10^{-3}$ (1/s), $[A_0]$=10nM, and $[R_0]$=10nM. The solid line, dot line (with squares) and dashed line (with Δ) denote, respectively, the predictions of the well-mixed model, the equilibrium pre-mixed model, and the non-equilibrium pre-mixed model.

10. The signal's amplitude $S\text{-}S_0$ as a function of the reporter particles' concentration. $k_{a1}=k_{a2}=k_{a3}=k_{a4}=10^6$ (1/MS), $k_{d1}=k_{d2}=k_{d3}=10^{-3}$(1/s), $[A_0]$=10nM, and $[R_0]$=10nM. The solid line, the dot line (with squares) and the dashed line (with Δ) denote, respectively, the predictions of the well-mixed model, the equilibrium pre-mixed model, and the non-equilibrium pre-mixed model.

11. The normalized signal $\left(\overline{S}-S_0\right)/\left(\overline{S}_{\max}-S_0\right)$ is depicted as a function of the normalized reporter particle concentration $[P_0]/[P_{0c}]$. The solid line, dashed line, and circles, correspond, respectively, to the premixed and unequlibrated **(PMU)** model predictions, the well-mixed (**PMW)** model predictions, and experimental data from Fig. 2B in [12].

12. The contrast index *DS* as a function of the concentration of immobilized ligands. $k_{a1}=k_{a2}=k_{a3}=k_{a4}=10^6$ (1/MS), $k_{d1}=k_{d2}=k_{d3}=k_{d4}=10^{-3}$ (1/s), $[A_0]$=10nM, and $[P_0]$=10nM. The

solid line, dot line (with squares) and dash line (with Δ) denote, respectively, the predictions of the well-mixed model, the equilibrium pre-mixed model, and the non-equilibrium pre-mixed model.

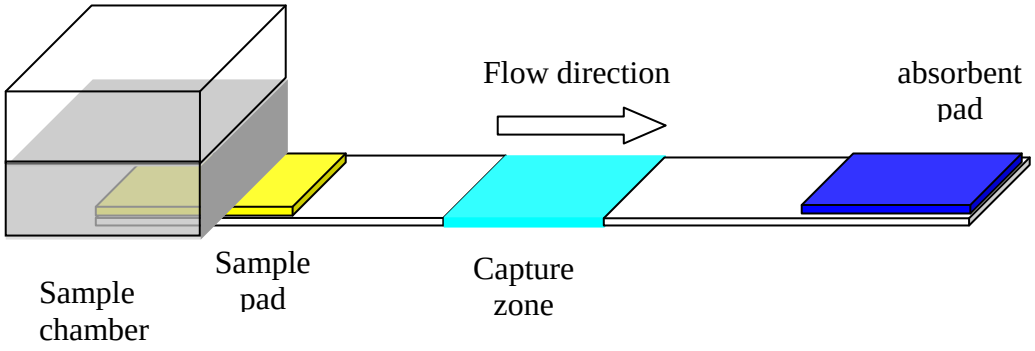

Fig.1: A schematic description of the lateral flow bio-detector. A mixture of target analyte A and reporter particles P migrate by capillary force up the membrane towards the capture zone where ligands are immobilized.

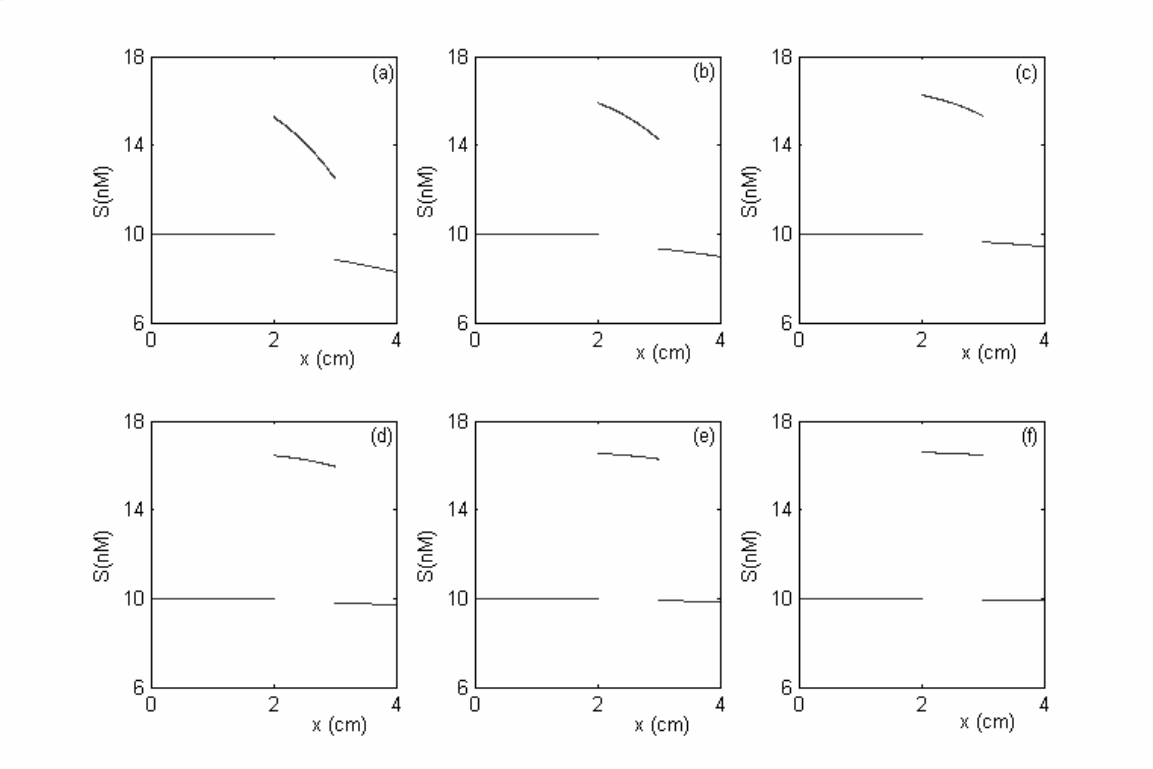

Fig. 2: The signal S as a function of the spatial coordinate x when a pre-mixed solution at equilibrium conditions is introduced into the membrane. $k_{a1}=k_{a2}=k_{a3}=k_{a4}=10^6$ (1/MS), $k_{d1}=k_{d2}=k_{d3}=k_{d4}=10^{-3}$ (1/s), $[A_0]=[P_0]=[R_0]$=10nM. t=4(a), 5(b), 6(c), 7(d), 8(e), and 9(f) min.

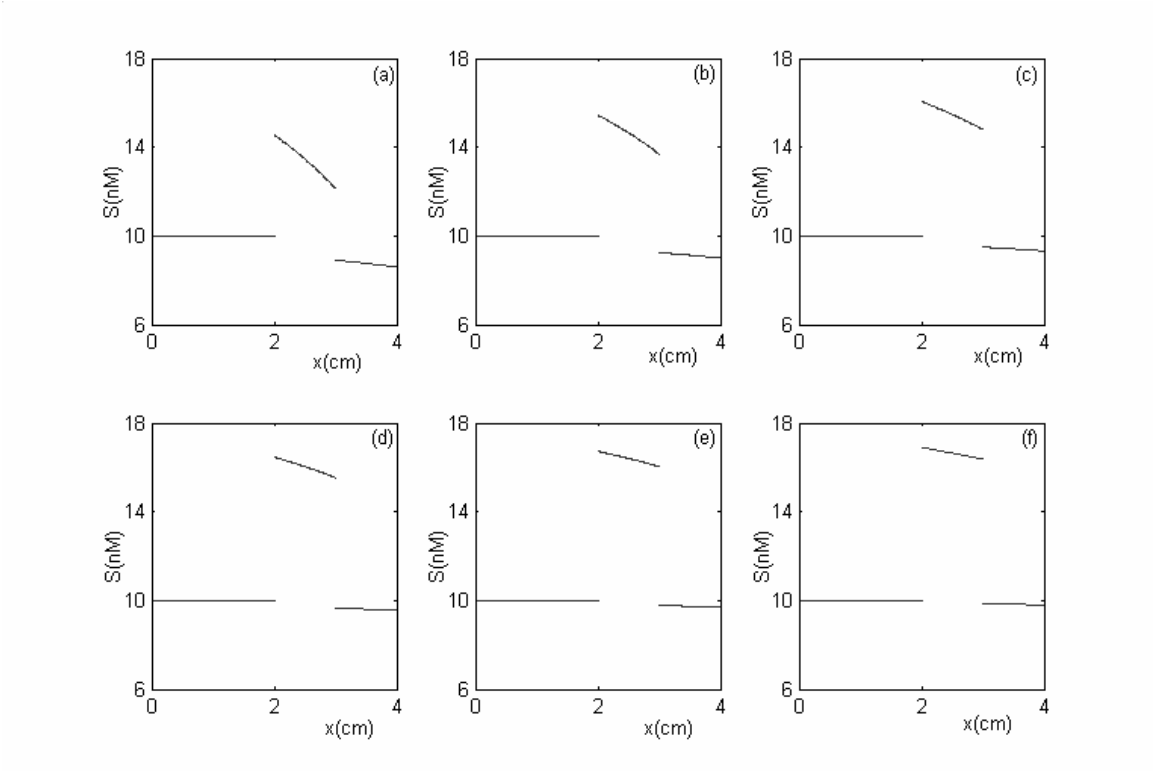

Fig. 3: The signal S as a function of the spatial coordinate x when a non-equilibrium, pre-mixed solution is introduced into the membrane. $k_{a1}=k_{a2}=k_{a3}=k_{a4}=10^6$ (1/MS), $k_{d1}=k_{d2}=k_{d3}=k_{d4}=10^{-3}$ (1/s), and $[A_0]=[P_0]=[R_0]$=10nM. t=4(a), 5(b), 6(c), 7(d), 8(e), and 9(f) min.

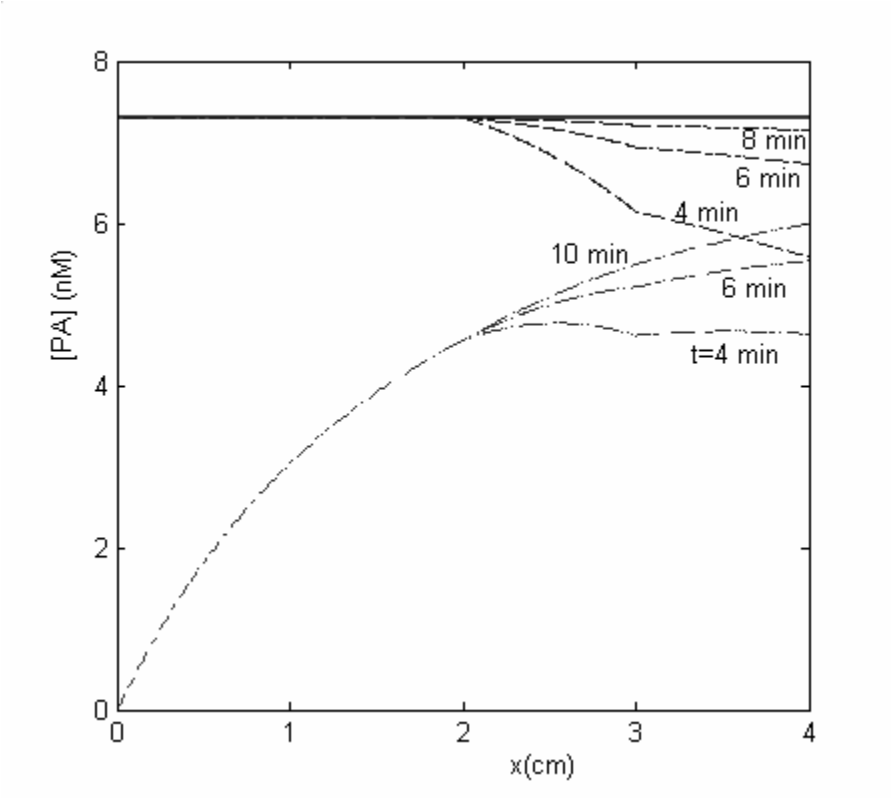

Fig.4: The concentration [*PA*] as a function of *x* for **PME** (dash lines), **PMU** (dash-dot lines) and **PMW** (solid line) conditions. $k_{a1}=k_{a2}=k_{a3}=k_{a4}=10^{6}$ (1/MS), $k_{d1}=k_{d2}=k_{d3}=k_{d4}=10^{-3}$ (1/s), and $[A_0]=[P_0]=[R_0]$=10nM.

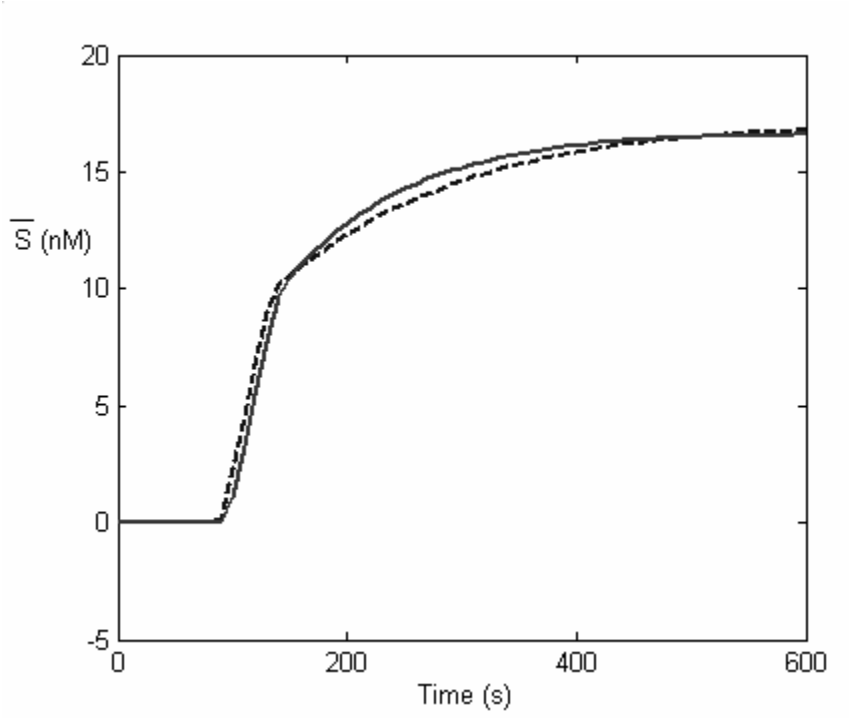

Fig.5: The average concentration $\overline{S}$ in the capture zone as a function of time for equilibrium pre-mixed (solid line) and non-equilibrium pre-mixed (dashed line) conditions. $k_{a1}=k_{a2}=k_{a3}=k_{a4}=10^6$ (1/MS), $k_{d1}=k_{d2}=k_{d3}=k_{d4}=10^{-3}$ (1/s), and $[A_0]=[P_0]=[R_0]$=10nM.

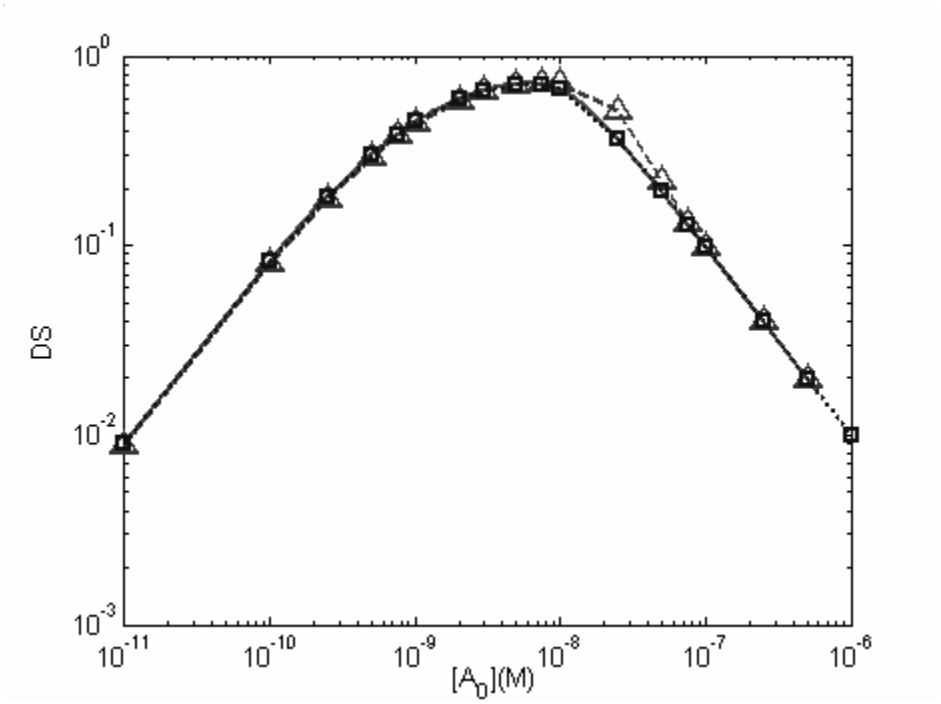

Fig. 6: The contrast index DS as a function of the target analyte concentration. $k_{a1}=k_{a2}=k_{a3}=k_{a4}=10^{6}$ (1/MS), $k_{d1}=k_{d2}=k_{d3}=k_{d4}=10^{-3}$ (1/s), $[P_0]$=10nM, and $[R_0]$=10nM. The solid line, dot line (with squares) and dashed line (with Δ) denote, respectively, the predictions of the well-mixed model, the equilibrium pre-mixed model, and the non-equilibrium pre-mixed model.

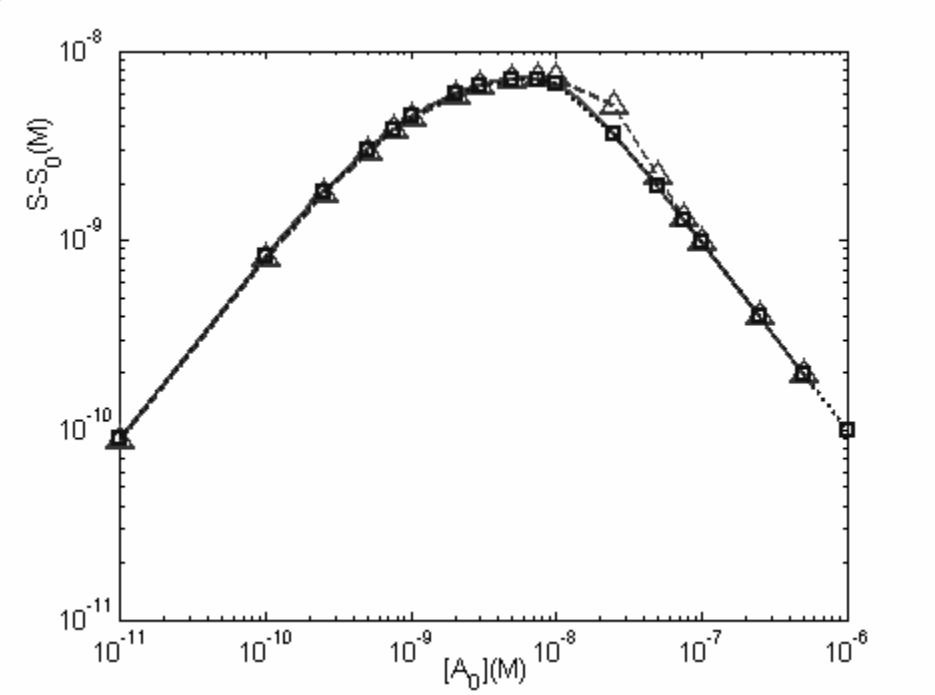

Fig. 7: The signal's amplitude $S\text{-}S_0$ as a function of the target analyte concentration. $k_{a1}=k_{a2}=k_{a3}=k_{a4}=10^6$ (1/MS), $k_{d1}=k_{d2}=k_{d3}=k_{d4}=10^{-3}$ (1/s), $[P_0]$=10nM, and $[R_0]$=10nM. The solid line, dot line (with squares) and dashed line (with Δ) denote, respectively, the predictions of the well-mixed model, the equilibrium pre-mixed model, and the non-equilibrium pre-mixed model.

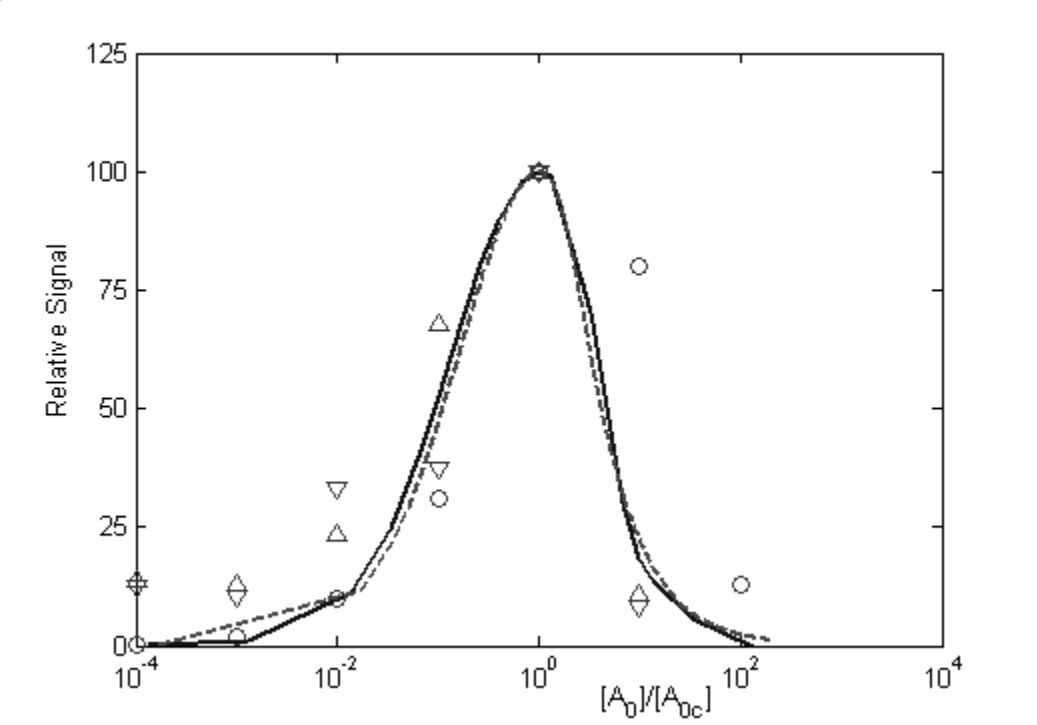

Fig. 8: The normalized signal $\left(\overline{S} - S_0\right)/\left(\overline{S}_{\max} - S_0\right)$ is depicted as a function of the normalized target analyte concentration $[A_0]/[A_{0c}]$. The solid line, dashed line, circles, upright triangles, and inverted triangles correspond, respectively, to premixed and unequlibrated (**PMU)** model predictions, well-mixed (**PMW)** model predictions, experimental data from Fig. 2c in [12], experimental data from Fig. 4 (SR membrane) in [19] and experimental data from Fig. 4 (SX membrane) in [19].

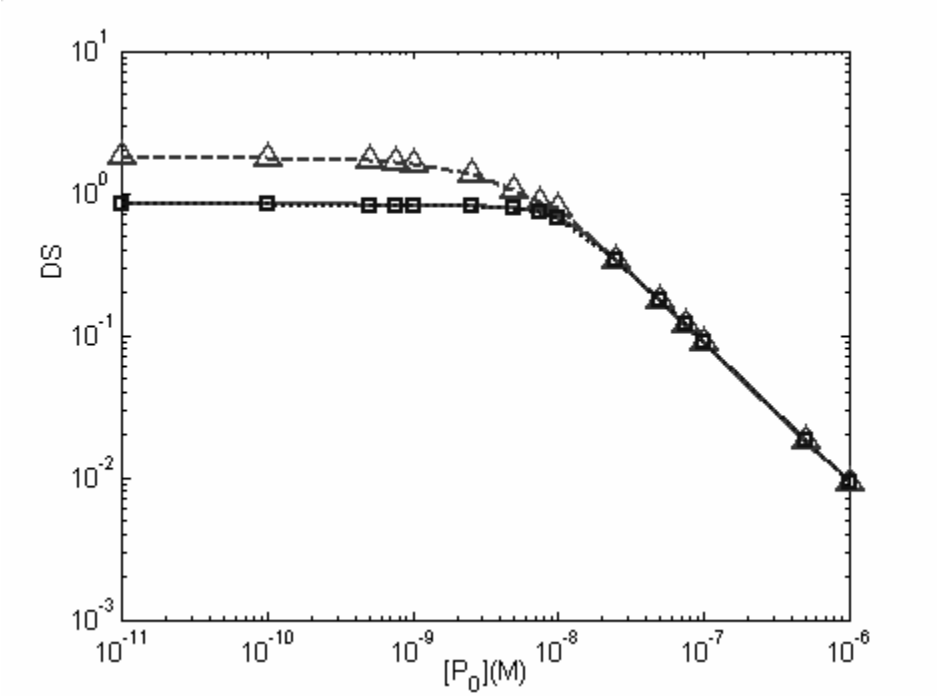

Fig. 9: The contrast index *DS* as a function of the reporter particles' concentration. $k_{a1}=k_{a2}=k_{a3}=k_{a4}=10^6$ (1/MS), $k_{d1}=k_{d2}=k_{d3}=k_{d4}=10^{-3}$ (1/s), $[A_0]$=10nM, and $[R_0]$=10nM. The solid line, dot line (with squares) and dashed line (with Δ) denote, respectively, the predictions of the well-mixed model, the equilibrium pre-mixed model, and the non-equilibrium pre-mixed model.

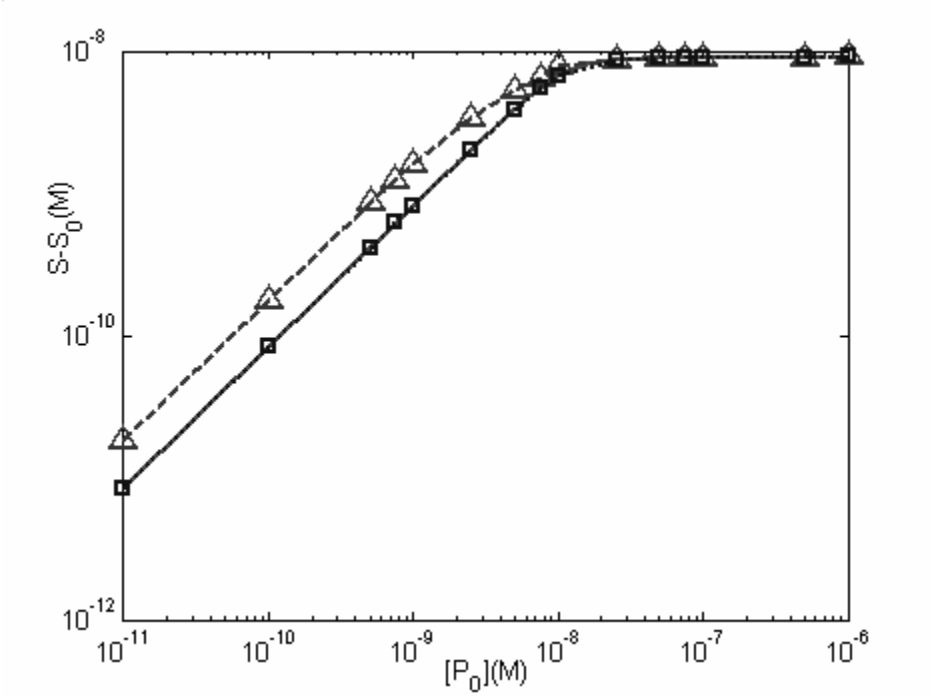

Fig. 10: The signal's amplitude $S\text{-}S_0$ as a function of the reporter particles' concentration. $k_{a1}=k_{a2}=k_{a3}=k_{a4}=10^6$ (1/MS), $k_{d1}=k_{d2}=k_{d3}=10^{-3}$(1/s), $[A_0]$=10nM, and $[R_0]$=10nM. The solid line, the dot line (with squares) and the dashed line (with Δ) denote, respectively, the predictions of the well-mixed model, the equilibrium pre-mixed model, and the non-equilibrium pre-mixed model.

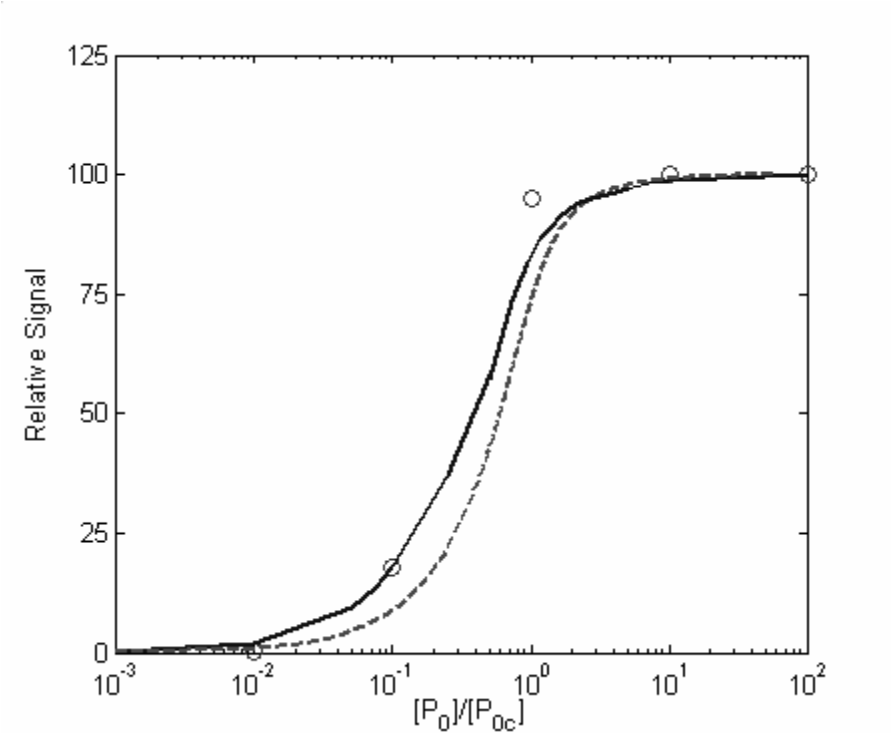

Fig. 11: The normalized signal $\left(\overline{S} - S_0\right)/\left(\overline{S}_{\max} - S_0\right)$ is depicted as a function of the normalized reporter particle concentration $[P_0]/[P_{0c}]$. The solid line, dashed line, and circles, correspond, respectively, to the premixed and unequlibrated (**PMU)** model predictions, the well-mixed (**PMW)** model predictions, and experimental data from Fig. 2B in [12].

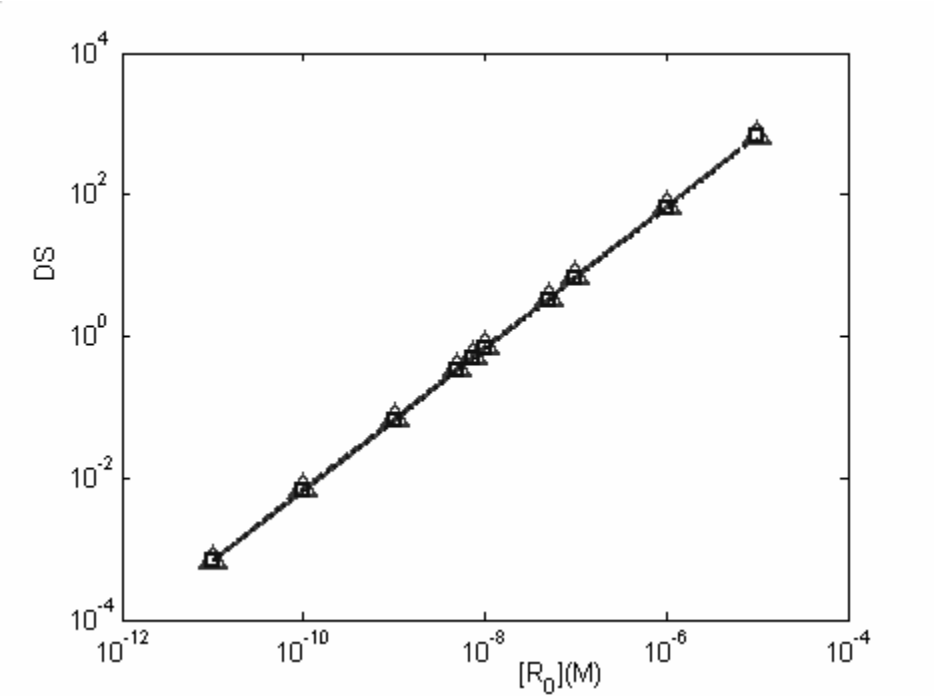

Fig. 12: The contrast index *DS* as a function of the concentration of immobilized ligands. $k_{a1}=k_{a2}=k_{a3}=k_{a4}=10^{6}$ (1/MS), $k_{d1}=k_{d2}=k_{d3}=k_{d4}=10^{-3}$ (1/s), $[A_0]$=10nM, and $[P_0]$=10nM. The solid line, dot line (with squares) and dash line (with Δ) denote, respectively, the predictions of the well-mixed model, the equilibrium pre-mixed model, and the non-equilibrium pre-mixed model.